Received: 25 December 2022 | Revised: 15 January 2023 | Accepted: 28 January 2023

https://doi.org/10.56946/jce.v1i02.104

Journal of Chemistry and Environment

Research article

Synthesis of bimetallic iron ferrite and its applications in alcohol fuel cell

Qurat-ul-Ain[1], Suqqyana Fazal[1], Fawad Ahmad[1*]

[1]Department of Chemistry, University of Wah, Wah Cantt, Postal Code 47040, Punjab, Pakistan

Correspondence: fawad.ahmad@uow.edu.pk

Abstract

Fuel cell is a clean, safe, eco-friendly source of energy as an alternative to already existing energy resources like incineration of fossil fuel. Efficiency of fuel cell is high when platinum is used as an electrode material for both anode and cathode. However, it is very expensive metal. Bimetallic Iron Ferrite (BMIF) has shown better EOR activity considering onset potential, mass activity when compared with noble metal catalyst but it is economical as compared to Pt. XRD reveals the conformation of BMIF and its purity. FTIR before and after electrochemical analysis has confirmed the retainment of its structure. However, it hasn't shown good activity for MOR in any parameter i-e Tafel slope value, mass activity and onset potential comparatively.

Keywords: EOR, MOR, Tafel slope, Onset potential, Electrocatalyst

Graphical Abstract:

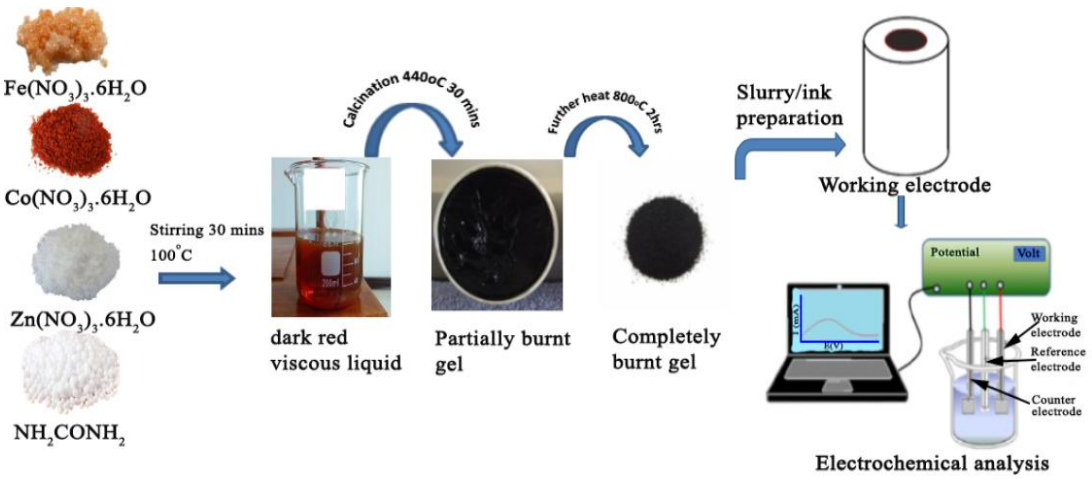

1.Introduction

One of the major issues that humanity is facing today is related to energy crises. Currently, incineration of fossil fuel is the major resource to meet the energy demands. However, this approach is not an environment friendly approach as it results in emission of harmful greenhouse gases and many other environmental perturbations [1]. Hence, there is a need of some alternative of already existing energy resources i-e electric batteries, fuel cell etc. The need of recharging, short life span due to charging and discharging cycles, draining dead batteries in open atmosphere, cost of electric batteries limit their use. As far as fuel cell is concerned, it is clean, reliable, efficient, sustainable, eco-friendly source of energy. Unlike batteries are thrown away, fuel cell is able to perform its function as long as fuel is provided. In hydrogen fuel cell (HFCs)

electricity up to 39.39 kWh/Kg^{-1} can be produced which super cede the energy density of many batteries [2]. Combustion engine convert fuel's chemical energy into mechanical energy which when pass through generator convert into electrical energy. In fuel cell chemical energy is converted into electrical energy precisely but without any harmful gas emission. The efficiency of fuel cell is high almost 60-65% in comparison to combustion engine i.e. 25-30%. In comparison to HFCs, DEFCs are more preferable because of less toxicity of ethanol, its immense production from biomass fermentation [3], its energy density is high 6.34 kWhL^{-1} as compared to hydrogen 0.53 kWhL^{-1} [4]. DAFCs use alcohol as a fuel i-e ethanol, methanol etc. Combinely, AFCs (Alkaline fuel cells) have higher current density, low corrosion rate, low cost [5]. The energy density of ethanol is very less (24 MJdm^{-3}) as compared to gasoline (34.2 MJdm^{-3}). However, efficiency factor of ethanol can be mitigated by its low cost and efficient production from biomass fermentation as compared to gasoline[6]. When Platinum or palladium is used as a catalyst for both the electrodes in fuel cell, its efficiency is very high. However, platinum is a very expensive metal and according to DOE 56% cost of fuel cell is just because of platinum based catalyst [7] .Numerous studies have been done by researchers to find some catalyst that is less expensive than platinum but its efficiency should be comparative to it [8]. In this context bimetallic and trimetallic oxides have shown better activity.

In present work, considering platinum free approach Bimetallic Iron Ferrite (BMIF) material or Cobalt Zinc Iron Ferrite material has been tested for both EOR and MOR. For EOR it has shown good activity comparative to platinum however not a very good catalyst considering MOR. The catalytic activity is determined using parameters i.e. Tafel slope value, onset potential, current density and mass activity.

2. Chemicals and methods:

2.1. Synthesis of catalyst:

Bimetallic Iron Ferrite (BMIF) or Cobalt zinc ferrite ($CoZnFe_2O_4$) particles were prepared using sol-Gel Combustion methodology. The reactants used were Fe $(NO_3)_3.9H_2O$, $Z(NO_3)_3.6H_2O$, $Co(NO_3)_3.6H_2O$. The concentration and amount of these reactants required is given in (Table 1).

All the above solutions are mixed in a proper stoichiometric amount followed by stirring for about half an hour and heating at 100^{o}C until a dark viscous gel like thick liquid is formed. This viscous liquid is then kept in furnace to further raise the temperature up to 440^{o}C for about half an hour. At this point, complete ignition of gel occurred. Temperature was further raised up to 800^{o}C for 2hrs and now proper incorporation of transition metals inside spinel ferrite crystalline structure takes place [9]. After that, burnt gel was ground into fine powder using pestle and mortar. Washing of prepared material was done using ethanol and water. Finally, the drying of product takes place at 100^{o}C in oven and then it was kept in dry place to study its electrochemical properties.

2.2. Catalyst Ink preparation:

After the synthesis of catalyst, in order to check its electrochemical activity we have to prepare the working electrode. First of all, we have prepared slurry or ink comprising Nafion membrane (as a binder), (isopropanol and ethanol 1:3) as a solvent, $CoZnFe_2O_4$ as a catalyst. The ratio among these three components is 1:1:1000 respectively [10]. After sonication for about 15-20 minutes a homogenous slurry will be formed. An ink drop was pasted on glassy carbon electrode (geometric surface area 0.07 cm^{-2}) followed by drying in open air. After complete drying, working electrode is now ready for electrochemical analysis.

3. Catalyst characterization:

3.1: SEM:

Fig 1 (A, B) shows particles are neither exactly spherical nor of any other definite shape when observed at scale of 1µm and 5µm. The relative distribution curves shows that the particle's size lies in the range of 0.08 to 0.3±0.02 µm.

Table 1. List of Chemicals for BMIF Synthesis

Sr. No	Chemical	Concentration (M)	Molecular Formula	% Purity
1	Iron(III) nitrate Nano hydrate	2	$Fe(NO_3)_3.9H_2O$	98
2	Cobaltous (II) nitrate Hex hydrate	0.5	$Co(NO_3)_2.6H_2O$	98
3	Zinc(II) nitrate Hex hydrate	0.5	$Zn(NO_3)_2.6H_2O$	95
4	Urea	6.67	NH_2CONH_2	98

Table 2: Current density of different anodic catalyst reported in literature [11].

Anodic catalyst	Electrolyte	Current density($mAcm^{-2}$)
Pd/G	1M KOH+1M Ethanol	0.8
Pd-Sn/C	same	1.4
Pd-Sn-Ni/C	same	2.25
Pt-vulcan	0.1M NaOH+1M Ethanol	0.5
Pt_3-Sn/vulcan	same	1
Pt-Sn Vulcan	same	2.25
Pd/MnO_2/vulcan	0.2M KOH +1M Ethanol	0.91
Pd-Ni/MnO_2/vulcan	same	1.46
Pd-Ni-Fe/MnO_2/vulcan	same	3.03
Our material	0.5M NaOH+1M Ethanol	1.1757
PdCo/C	Same	48
Pd/C (commercial)		27

.

However, when analyzed at more magnified 5 µm scale, particles were found to be of spherical shape but they were in agglomerated state due to magnetic interactions among them [12, 13]. As far as surface is concerned, it does not appear homogenous due to the polydisperse system (non-uniform size distribution). At some areas, pores are also observed. This might be due to liberation of gases at high temperature which have loosen the crystalline structure a little bit [14].

3.2. XRD:

Our sample material have shown cubic spinel structure (Figure 2) in accordance with literature reported data [15]. Spineal structure has been confirmed through the strongest or the intense peak obtained for (311) plane at $2\theta = 35^o$ [16, 17]. No extra peaks were observed in XRD plot showing high purity of our sample material [18]. Crystallite size has also been calculated using sherrer equation (0.315 µm), which is in accordance with result obtained from SEM analysis (0.08-0.3 µm). A crystallite consist of many particles, hence crystallite size is greater than particle size [19].

3.3. FTIR:

FTIR spectra (Figure 3, 1.4) have shown how the cations are scattered in octahedral and tetrahedral sites? Spectra existing in finger print region (400 to 600 cm^{-1}) due to metal-oxygen stretching vibrations has confirmed the spinel structure of BMIF [20].The bands at high frequency are attributed to stretching vibration of (M_{tet}-O) while at low frequency is due to stretching vibration of (M_{oct}-O) [21]. As the bond length of tetrahedral complexes is shorter and hence their mode of vibration is high as compared to octahedral complexes [12].The weak broader bands appear near 3400 cm^{-1} and

peaks near 1600 cm^{-1} (Fig1.3) is due to adsorbed moisture on ferrite surface[22, 23]. H-O-H bending vibration of water show band near 3400 cm^{-1}. The peak near 1600 cm^{-1} is due to OH^- stretching vibrations [24, 25].

We have concluded from FTIR spectrum of BMIF that before and after electrochemical analysis (Figure 4), spinel structure remains persistent. All peaks are obtained in the same frequency range (400-600cm^{-1}) even after electrochemical analysis confirming the high structural stability of BMIF.

4. Electrochemical activity:

Cyclic voltammetry, linear sweep voltammetry are used to check electrochemical properties (EOR and MOR) of sample material.

Table 3: Mass activity of different Pd based electrocatalyst reported in literature

Metal catalyst	Mass activity($mAmg^{-1}$)	References
Pd/C	95 vs Hg/HgO	[26]
Pd/Bi-C	279	[27]
PdCo/C	105	[26]
Pd_2Ni_3/C	1.71	[28]

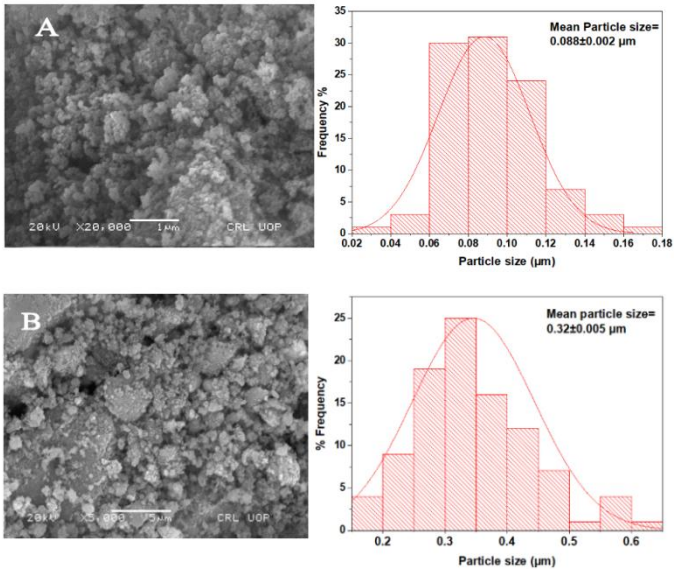

Figure 1: (A) BMIF SEM images at bar scale of 1µm and its relative distribution curve (B) BMIF SEM images at bar scale of 5µm and its relative distribution curve

4.1. Ethanol Oxidation Reaction (EOR):

Mechanism of EOR is a dual pathway C_1 and C_2 pathway [29],

C_1 (complete oxidation)

$$CH_3CH_2OH \rightarrow CO + CH_X \rightarrow CO_2 + 12e^-$$

C_2 (incomplete oxidation)

$$CH_3CH_2OH \rightarrow CH_3COOH + 4e^-$$

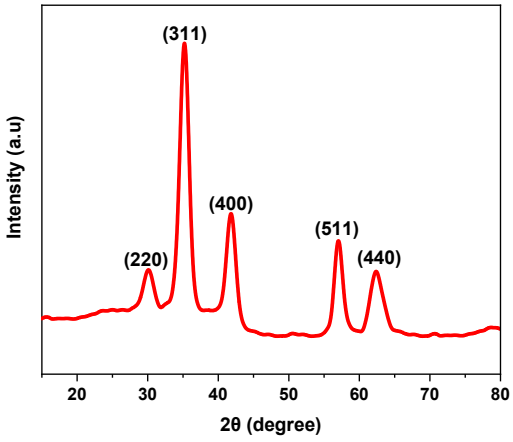

Figure 2: XRD plot for BMIF with maximum peak obtained at 2θ=35°

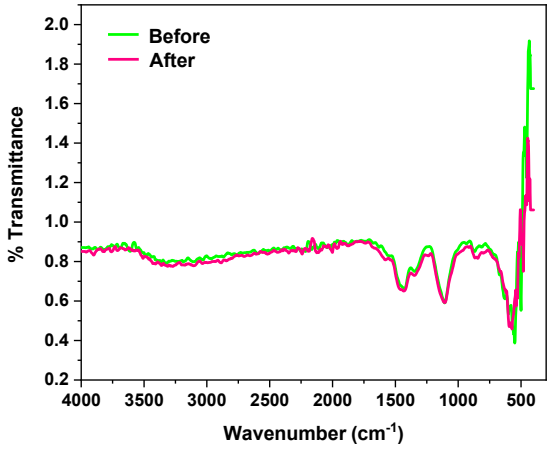

Figure 3: FTIR spectrum of BMIF before and after electrochemical analysis in range of 4000-400 cm^{-1}

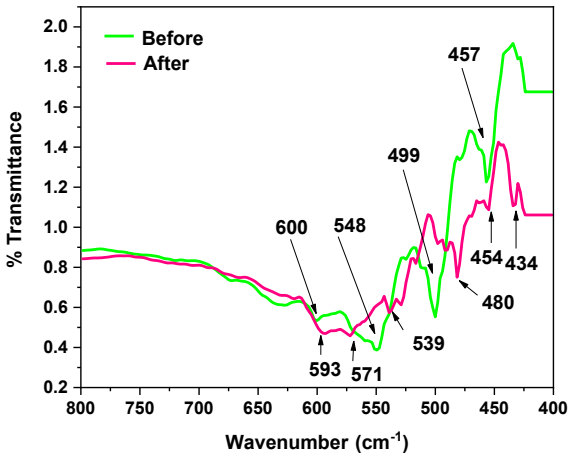

Figure 4: FTIR Spectrtum of BMIF before and after electrochemical analysis in finger print region (800-400 cm^{-1}).

At high pH (alkaline medium) there is great possibility of C_1pathway [30] as it is suggested that aldol condensation at alkaline medium supports C_1 pathway. Because the α hydrogen in CH_3 of acetaldehyde is slightly acidic, it is more prone to be attacked by (OH^-) [31]. Consequently, C-C bond is now slightly hindered and now it is facile to break this bond. This suggestion towards selectivity of C_1 pathway is further reinforced by the fact that the intermediates of this route i-e $CH_{x.ads}$ [32] and CO_{ads} [33] can easily be oxidized at low over potential in alkaline medium as compared to acidic one. We will determine the EOR catalytic activity of our sample material on the basis of following parameters.

Current density.

The current density calculated from the (Figure 5) at 1.5 V is (0.0823/0.07=1.1757 $mAcm^{-2}$).when we compared the current density for different anodic catalyst reported in literature , this value is found to be in accordance as shown in (Table 2).

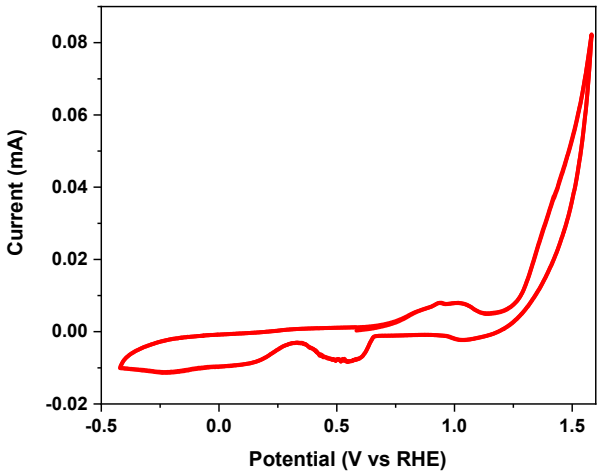

Figure 5: CV for BMIF at scan rate of 50 mVs^{-1}

Mass* activity*:

The mass activity of our material is calculated from (Figure 5) at 1.5V (0.0823/0.001=82.3 $mAmg^{-1}$) and at 0.9V (0.003517/0.001= 3.517 $mAmg^{-1}$) .The mass activity value reported in literature for other noble metal based catalyst is given in (Table1.3). The mass activity of BMIF is in good accordance with the reported values in literature for other noble catalyst.

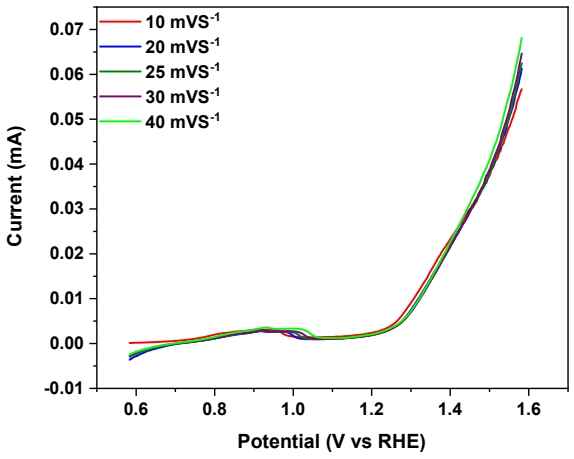

Figure 6: LSV curves for BMIF at different scan rate.

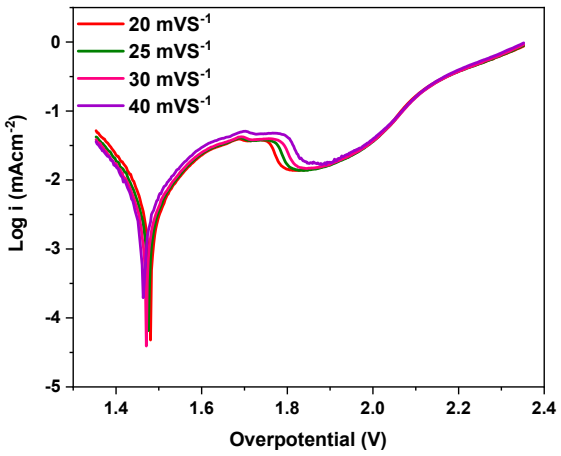

Figure 7: Tafel plot of BMIF for EOR at different scan rate.

Onset* potential*:

Onset potential is the difference between equilibrium potential and the applied potential [34]. Low value of onset potential is an indication of efficient metal for EOR [35, 36]. Table 5 shows the comparison of onset potential for BMIF with other catalyst containing noble metals.

Tafel slope value:

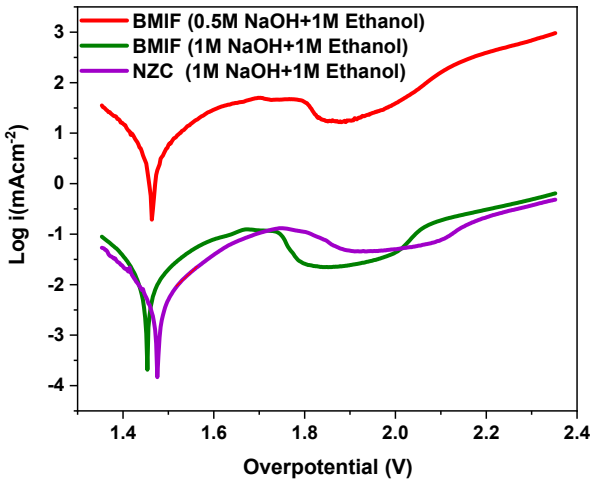

Figure 8: Tafel slope value of two electrocatalysts (BMIF and

NZC, NiZnCuO) for EOR in different electrolyte.

(Figure 8 , Table 7) shows that NZC (NiZn CuO) posses greater tafel slope value in comparison to BMIF showing its less activity as compared to BMIF.

We have seen that (Figure 6, Table 4), with increase in scan rate the current response increases in accordance with Randles Sevick equation.

$$i_p = 0.446nFAC^0\left(\frac{nF\nu D_o}{RT}\right)^{1/2} \qquad eq-1$$

All the observations from (Figure 6) are summarized in (Table 4).

Table 4: Numerical data showing current density of BMIF for EOR at different scan rate

Scan rate(mVs^{-1})	Onset potential(v)	Over-potential(V)	Current response(mA)	Current density($mAcm^{-2}$)
10	0.907	1.677	0.0033	0.046
20	0.916	1.686	0.00296	0.0416
25	0.919	1.689	0.00304	0.0428
30	0.921	1.691	0.0032	0.0450
40	0.922	1.692	0.0038	0.0535

Table 5: Onset potential for EOR of some other electro catalyst reported in literature:

Sr No;	Electrocatalyst	Onset potential(V vs RHE)	References	Over-potential(V)
1	Ni-Pd/ PVA	1.27	[37]	2.04
2	$Pt_{2.3}$-Ni/C	0.6	[38]	1.37
3	Ni-MnO_2	1.32	[39]	2.09
4	Pt	0	[40]	0
5	Cu_2O/PPy	1.45	[41]	2.22
6	Pt/MoS_2	0.67	[42]	1.44
7	Pt/C	1.36	[43]	2.13
8	Pd	0.9	[44]	1.67
9	Pt-CeO_2	1	[45]	1.77
10	Co-Bi@rGO	1.28	[46]	2.05
	Our work	**0.9**		**1.67**

Table 6: BMIF tafel slope value at different scan rate

Scan rate (mVs^{-1})	Tafel slope value ($Vdec^{-1}$)
20	6.408± 0.10522
25	6.961±0.1182
30	6.702±0.10082
40	6.907 ±0.077

At low scan rate (Figure 7) Tafel slope value is less showing best activity of catalyst (Table 6).

Table 7: Tafel slope for BMIF and NZC from (Figure 8)

Sample material	Electrolyte	Tafel slope value
BMIF	0.5M NaOH+1M Ethanol	7.748 ± 0.1334
BMIF	1M NaOH+1M Ethanol	7.127 ± 0.1080
NZC	same	8.465 ± 0.13128

Table 8: comparison of BMIF EOR activity with noble metal catalyst reported in literature.

Catalyst	Mass Activity ($mAmg^{-1}$)[47]	Tafel slope ($Vdec^{-1}$)
Pt/C at 0.45 V	4	0.619 [48]
Pd/C at 0.45V	25.4	0.182-0.195 [49, 50]
Pd based catalyst	-	0.12-0.17 [27, 51]
BMIF at 0.9V	3.517	6.9-7.7
BMIF at 1.5V	82.3	-

In a nutshell, BMIF is showing good mass activity comparative to Pt and Pd but at the expense of high potential. In terms of Tafel slope value our material is showing high value comparatively.

Table 9: Numerical data from BMIF LSV for MOR at different scan rate

Scan rate (mVs^{-1})	Onset potential (v)	Over potential (V)	Current response(mA)	Current density($mAcm^{-2}$)
20	0.9153	1.725	0.003259	0.04590
30	0.91094	1.720	0.002964	0.04174
40	0.9492	1.719	0.004302	0.06059
50	0.9547	1.7647	0.004971	0.07001

4.2. Methanol oxidation reaction (MOR):

The MOR mechanism suggested is as follows[52],

$$CH_3OH + H_2O \rightarrow 6H^+ + 6e^- + CO_2$$

The formal reduction potential for MOR reported in literature is -0.81 [53].

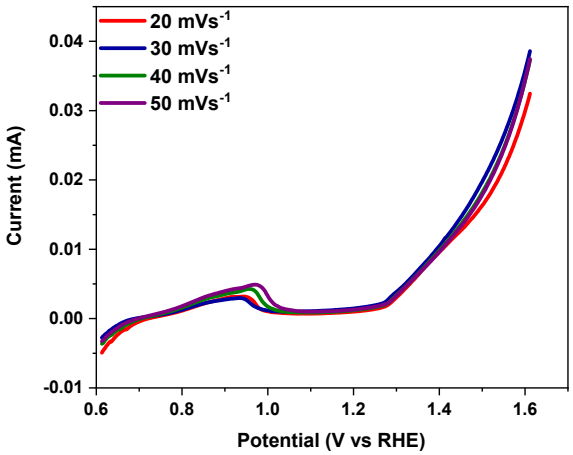

Figure 9: LSV curves of BMIF for MOR at different scan rate

Tafel slope value:

Smaller the Tafel slope value , greater will be the over potential and hence catalyst under study would be poor [54]with increasing scan rate anodic Tafel slope value and corrosion rate also increases [55]. (Figure 10, Table 10) gives information about Tafel slope value for MOR at different scan rate. Low scan rate is again the best option to obtain good activity of BMIF for MOR.

Onset potential:

Figure 9 shows LSV curves for MOR from where we can get useful information about current density and onset potential. BMIF has shown greater value of onset potential i-e 0.8 V (Table 9) in comparison to Pt i-e 0.4 V (Table 11)

Mass activity:

The value of limiting current obtained at 0.9 V from (Figure 9) is i_l= 0.005096 mA. The mass activity calculated is 5.095 $mAmg^{-1}$.(Table 9) much less than mass activity of Pt as mentioned in (Table 11).

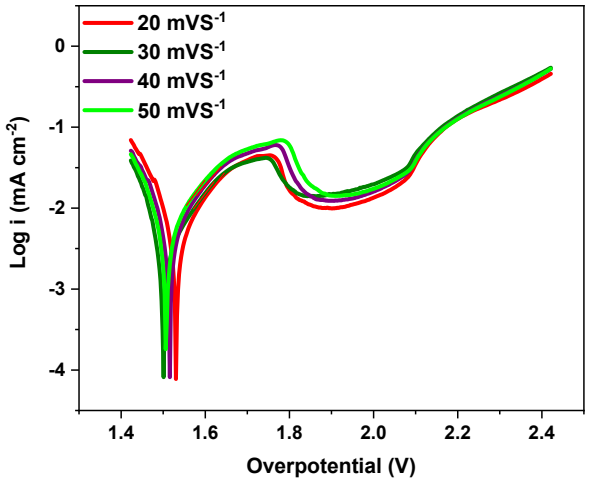

Figure 10 : BMIF Tafel slope value at different scan rate

In a nutshell, BMIF is showing good mass activity comparative to Pt and Pd but at the expense of high potential. In terms of Tafel slope value our material is showing high value comparatively.

Table 10: BMIF tafel slope value for MOR at different scan rate

Scan rate mVs^{-1}	Tafel slope value
20	6.725 ± 0.09
30	6.880 ±0.602
40	6.980 ±0.078
50	7.119 ±0.07

Table 11: comparison of BMIF MOR activity with noble metal catalyst reported in literature

Catalyst	Tafel slope ($Vdec^{-1}$)	Onset potential (V)	Mass activity($mAmg^{-1}$)
Pt/C	0.166[56]	0.448[57]	56[58]
BMIF	6.7-7.11	0.8	5.095

BMIF haven't shown good activity for MOR in any parameter (Table 11).

5. Conclusion:

We have determined the catalytic activity of BMIF for EOR and MOR on the basis of different parameters. Spinel structure of BMIF was analyzed from XRD and retainment of this crystalline structure even after electrochemical analysis was confirmed through FTIR analysis. In terms of EOR, Onset potential and mass activity values were found in accordance with the one reported for noble metal catalyst reported in literature. However, BMIF cannot be suggested as good catalyst for MOR in comparison to noble metal catalyst.

6. Future perspective:

- Effect of temperature on activity of catalyst
- Combination of BMIF with any carbonaceous material might enhance its activity for MOR
- Poisoning of electrode due to oxides of carbon produced as a result of EOR and MOR needs further study.

Authors Contribution

QA and FA has the main idea of the manuscript. QA and SF wrote the the manuscript. FA revised the manuscript and provide suggestions.

.Conflicts of Interest

The authors reported no potential conflict of interest.

Acknowledgment

This work is financially supported by Chemistry Department, University of Wah.

Data Availability statement

The data presented in this study are available on request from the corresponding author.

REFERENCES

1. Kannan, M., Current status, key challenges and its solutions in the design and development of graphene based ORR catalysts for the microbial fuel cell applications. Biosensors and Bioelectronics, 2016. **77**: p. 1208-1220.

2. Manoharan, Y., et al., Hydrogen fuel cell vehicles; current status and future prospect. Applied Sciences, 2019. **9**(11): p. 2296.
3. Vigier, F., et al., On the mechanism of ethanol electro-oxidation on Pt and PtSn catalysts: electrochemical and in situ IR reflectance spectroscopy studies. Journal of Electroanalytical Chemistry, 2004. **563**(1): p. 81-89.
4. Lamy, C., et al., Recent advances in the development of direct alcohol fuel cells (DAFC). Journal of Power Sources, 2002. **105**(2): p. 283-296.
5. Kamarudin, M., et al., Direct ethanol fuel cells. International journal of hydrogen energy, 2013. **38**(22): p. 9438-9453.
6. Akhairi, M. and S.K. Kamarudin, Catalysts in direct ethanol fuel cell (DEFC): An overview. International Journal of Hydrogen Energy, 2016. **41**(7): p. 4214-4228.
7. Saedi, L., et al., Oxygen Activation on Four-Atom Metal Clusters and Alloys. Journal of Structural Chemistry, 2020. **61**(4): p. 515-522.
8. Nie, Y., L. Li, and Z. Wei, Recent advancements in Pt and Pt-free catalysts for oxygen reduction reaction. Chemical Society Reviews, 2015. **44**(8): p. 2168-2201.
9. Das, I., et al., Synthesis of bimetallic iron ferrite CoO. 5ZnO. $5Fe_2O_4$ as a superior catalyst for oxygen reduction reaction to replace noble metal catalysts in microbial fuel cell. International Journal of Hydrogen Energy, 2018. **43**(41): p. 19196-19205.
10. Ahmad, F., et al., Boosting fuel cell catalysis by surface doping of W on Pd nanocubes. Chinese Journal of Catalysis, 2018. **39**(7): p. 1202-1209.
11. Kazan, E.S. and M. Bayramoğlu, Molybdenum compound cocatalyzed Ni-based anode electrocatalysts for EOR in alkaline media. International Journal of Energy Research, 2021. **45**(9): p. 12806-12824.
12. Tatarchuk, T., et al., Structural characterization and antistructure modeling of cobalt-substituted zinc ferrites. Journal of Alloys and Compounds, 2017. **694**: p. 777-791.
13. Borhan, A.I., et al., Cr^{3+} and Al^{3+} co-substituted zinc ferrite: Structural analysis, magnetic and electrical properties. Polyhedron, 2014. **70**: p. 110-118.
14. Tatarchuk, T., et al., Spinel cobalt (II) ferrite-chromites as catalysts for H_2O_2 decomposition: Synthesis, morphology, cation distribution and antistructure model of active centers formation. Ceramics International, 2020. **46**(17): p. 27517-27530.
15. Vaidyanathan, G. and S. Sendhilnathan, Characterization of $Co_{1-x}Zn_xFe_2O_4$ nanoparticles synthesized by co-precipitation method. Physica B: Condensed Matter, 2008. **403**(13-16): p. 2157-2167.
16. Betancourt-Galindo, R., O. Rodríguez-Fernández, and E. Medina-Rodríguez, Obtención de látex magnético mediante la técnica de polimerización en miniemulsión. Superficies y Vacío, 2004. **17**(1): p. 38-41.
17. Kim, Y.I., D. Kim, and C.S. Lee, Synthesis and characterization of $CoFe_2O_4$ magnetic nanoparticles prepared by temperature-controlled coprecipitation method. Physica B: Condensed Matter, 2003. **337**(1-4): p. 42-51.
18. Bohara, R., et al., Synthesis of functionalized CoO. 5ZnO. $5Fe_2O_4$ nanoparticles for biomedical

applications. Journal of Magnetism and Magnetic Materials, 2015. **378**: p. 397-401.

19. Sumari, S., A. Roesyadi, and S. Sumarno, Effects of ultrasound on the morphology, particle size, crystallinity, and crystallite size of cellulose. Scientific Study & Research. Chemistry & Chemical Engineering, Biotechnology, Food Industry, 2013. **14**(4): p. 229.
20. Kaur, H., et al., Structural, thermal and magnetic investigations of cobalt ferrite doped with Zn^{2+} and Cd^{2+} synthesized by auto combustion method. Journal of Magnetism and Magnetic Materials, 2019. **474**: p. 505-511.
21. Slatineanu, T., et al., Synthesis and characterization of nanocrystalline Zn ferrites substituted with Ni. Materials Research Bulletin, 2011. **46**(9): p. 1455-1460.
22. Kannan, K., et al., Structural and biological properties with enhanced photocatalytic behaviour of CdO-MgO nanocomposite by microwave-assisted method. Optik, 2020. **204**: p. 164221.
23. Revathi, V. and K. Karthik, Physico-chemical properties and antibacterial activity of Hexakis (Thiocarbamide) Nickel (II) nitrate single crystal. Chemical Data Collections, 2019. **21**: p. 100229.
24. Suresh, S., et al., Green synthesis of copper oxide nanostructures using Cynodon dactylon and Cyperus rotundus grass extracts for antibacterial applications. Ceramics International, 2020. **46**(8): p. 12525-12537.
25. Harris, R.I., Discussion of "The annual rate of independent events for the analysis of extreme wind speed" by Alessio Torrielli, Maria Pia Repetto & Giovanni Solari. Journal of Wind Engineering and Industrial Aerodynamics, 2017. **100**(164): p. 174-178.
26. Sankar, S., et al., Cobalt-Modified Palladium Bimetallic Catalyst: A Multifunctional Electrocatalyst with Enhanced Efficiency and Stability toward the Oxidation of Ethanol and Formate in Alkaline Medium. ACS Applied Energy Materials, 2018. **1**(8): p. 4140-4149.
27. Cai, J., Y. Huang, and Y. Guo, Bi-modified Pd/C catalyst via irreversible adsorption and its catalytic activity for ethanol oxidation in alkaline medium. Electrochimica Acta, 2013. **99**: p. 22-29.
28. Zhang, Z., et al., Pd–Ni electrocatalysts for efficient ethanol oxidation reaction in alkaline electrolyte. International Journal of Hydrogen Energy, 2011. **36**(20): p. 12686-12697.
29. Lan, B., et al., Ethanol Electrooxidation on Rhodium–Lead Catalysts in Alkaline Media: High Mass Activity, Long-Term Durability, and Considerable CO_2 Selectivity. Small, 2020. **16**(40): p. 2004380.
30. Rao, V., C. Cremers, and U. Stimming, Investigation of the ethanol electro-oxidation in alkaline membrane electrode assembly by differential electrochemical mass spectrometry. Fuel Cells, 2007. **7**(5): p. 417-423.
31. Guthrie, J.P., Rate-equilibrium correlations for the aldol condensation: an analysis in terms of Marcus theory. Journal of the American Chemical Society, 1991. **113**(19): p. 7249-7255.
32. Lai, S.C. and M.T. Koper, Ethanol electro-oxidation on platinum in alkaline media. Physical Chemistry Chemical Physics, 2009. **11**(44): p. 10446-10456.

33. García, G. and M.T. Koper, Stripping voltammetry of carbon monoxide oxidation on stepped platinum single-crystal electrodes in alkaline solution. Physical Chemistry Chemical Physics, 2008. **10**(25): p. 3802-3811.
34. Pegis, M.L., et al., Standard reduction potentials for oxygen and carbon dioxide couples in acetonitrile and N, N-dimethylformamide. Inorganic Chemistry, 2015. **54**(24): p. 11883-11888.
35. Rostami, H., A.A. Rostami, and A. Omrani, An electrochemical method to prepare of Pd/Cu_2O/MWCNT nanostructure as an anode electrocatalyst for alkaline direct ethanol fuel cells. Electrochimica Acta, 2016. **194**: p. 431-440.
36. Gu, Y., et al., A ternary nanocatalyst of Ni/Cr/Co oxides with high activity and stability for alkaline glucose electrooxidation. Electrochimica Acta, 2016. **192**: p. 296-302.
37. Mohamed, I.M., et al., Electrocatalytic behavior of a nanocomposite of Ni/Pd supported by carbonized PVA nanofibers towards formic acid, ethanol and urea oxidation: A physicochemical and electro-analysis study. Applied Surface Science, 2018. **435**: p. 122-129.
38. Sulaiman, J.E., et al., Pt–Ni octahedra as electrocatalysts for the ethanol electro-oxidation reaction. ACS Catalysis, 2017. **7**(8): p. 5134-5141.
39. Nakayama, M., K. Suzuki, and K. Fujii, Single-ion catalyst of Ni^{2+} anchored in the interlayer space of layered MnO_2 for electro-oxidation of ethanol in alkaline electrolyte. Electrochemistry Communications, 2019. **105**: p. 106492.
40. Wang, B., et al., Electrocatalytic oxidation of small molecule alcohols over Pt, Pd, and Au catalysts: The effect of alcohol's hydrogen bond donation ability and molecular structure properties. Catalysts, 2019. **9**(4): p. 387.
41. El Attar, A., et al., Preparation and characterization of copper oxide particles/polypyrrole (Cu_2O/PPy) via electrochemical method: Application in direct ethanol fuel cell. International Journal of Hydrogen Energy, 2020. **45**(15): p. 8887-8898.
42. Wang, J., et al., MoS_2 nanoflower supported Pt nanoparticle as an efficient electrocatalyst for ethanol oxidation reaction. International Journal of Hydrogen Energy, 2019. **44**(31): p. 16411-16423.
43. Ma, K.-B., et al., Direct ethanol fuel cells with superior ethanol-tolerant nonprecious metal cathode catalysts for oxygen reduction reaction. ACS Sustainable Chemistry & Engineering, 2018. **6**(6): p. 7609-7618.
44. Zhang, R.-L., et al., One-step aqueous synthesis of hierarchically multi-branched PdRuCu nanoassemblies with highly boosted catalytic activity for ethanol and ethylene glycol oxidation reactions. Applied Surface Science, 2020. **506**: p. 144791.
45. Murphin Kumar, P.S., et al., Pt nanoparticles supported on mesoporous CeO_2 nanostructures obtained through green approach for efficient catalytic performance toward ethanol electro-oxidation. ACS Sustainable Chemistry & Engineering, 2017. **5**(12): p. 11290-11299.
46. Munde, A.V., et al., Electrocatalytic ethanol oxidation on cobalt–bismuth nanoparticle-decorated reduced graphene oxide (Co–Bi@

rGO): reaction pathway investigation toward direct ethanol fuel cells. The Journal of Physical Chemistry C, 2021. **125**(4): p. 2345-2356.

47. Ma, L., D. Chu, and R. Chen, Comparison of ethanol electro-oxidation on Pt/C and Pd/C catalysts in alkaline media. International Journal of Hydrogen Energy, 2012. **37**(15): p. 11185-11194.
48. Pushkarev, A.S., et al., Pt/C and Pt/SnOx/C catalysts for ethanol electrooxidation: Rotating disk electrode study. Catalysts, 2019. **9**(3): p. 271.
49. Tripković, A., K.D. Popović, and J. Lović, The influence of the oxygen-containing species on the electrooxidation of the C1–C4 alcohols at some platinum single crystal surfaces in alkaline solution. Electrochimica Acta, 2001. **46**(20-21): p. 3163-3173.
50. Shen, S., T. Zhao, and J. Xu, Carbon supported PtRh catalysts for ethanol oxidation in alkaline direct ethanol fuel cell. international journal of hydrogen energy, 2010. **35**(23): p. 12911-12917.
51. Wang, M., W. Liu, and C. Huang, Investigation of PdNiO/C catalyst for methanol electrooxidation. International Journal of Hydrogen Energy, 2009. **34**(6): p. 2758-2764.
52. Yuda, A., A. Ashok, and A. Kumar, A comprehensive and critical review on recent progress in anode catalyst for methanol oxidation reaction. Catalysis Reviews, 2022. **64**(1): p. 126-228.
53. Yu, E.H., U. Krewer, and K. Scott, Principles and materials aspects of direct alkaline alcohol fuel cells. Energies, 2010. **3**(8): p. 1499-1528.
54. Qin, Y.-H., et al., Effect of carbon nanofibers microstructure on electrocatalytic activities of Pd electrocatalysts for ethanol oxidation in alkaline medium. International Journal of Hydrogen Energy, 2010. **35**(15): p. 7667-7674.
55. Prajitno, D.H. Effects of scan rate on the corrosion behavior SS-304 stainless steel in the nanofluid measured by Tafel polarization methods. in AIP Conference Proceedings. 2015. AIP Publishing LLC.
56. Fang, Y.-H. and Z.-P. Liu, First principles Tafel kinetics of methanol oxidation on Pt (111). Surface Science, 2015. **631**: p. 42-47.
57. Zhang, Z., et al., Single-atom catalyst for high-performance methanol oxidation. Nature communications, 2021. **12**(1): p. 1-9.
58. Wang, Y., et al., Promoting effect of nickel hydroxide on the electrocatalytic performance of Pt in alkaline solution. Dalton Transactions, 2018. **47**(24): p. 7975-7982.

How to cite this article:

Ain Q, Fazal S, Ahmad F. (2023). Synthesis of bimetallic iron ferrite and its applications in alcohol Fuel cell. Journal of Chemistry and Environment. 2(1).p.1-13